International Journal of Innovative Computing, Information and Control
Volume **8**, Number **3(B)**, March **2012**

ICIC International ©2012 ISSN 1349-4198
pp. **2399–2413**

UKF-BASED COLLISION DETECTION AND CONTROL OF PARALLEL-STRUCTURED TWO-LINK FLEXIBLE MANIPULATORS

Yuichi Sawada[1], Junki Kondo[2] and Yusuke Watanabe[3]

[1]Division of Mechanical and System Engineering
Kyoto Institute of Technology
Matsugasaki, Sakyo, Kyoto 606-8585, Japan
sawada@kit.ac.jp

[2]Department of Servo Motor Manufacturing
Mitsubishi Electric Corporation Nagoya Works
5 Yada-minami, Higashi, Nagoya 461-8670, Japan

[3]Shiga Technical Center, Second Development Department
NIDEC Corporation
248 Nakajuku, Aisho-cho, Echi-gun, Shiga 529-1385, Japan

Received March 2011; revised July 2011

Abstract. *A method based on an unscented Kalman filter is presented for collision detection and control of parallel-structured two-link flexible manipulators. The exact dynamics of parallel-structured two-link flexible manipulators is described by nonlinear partial and ordinary differential equations having considerable complexity. Here, manipulators are modeled approximately by a two-link flexible manipulator consisting of a pair of flexible beams under the same boundary conditions as the original system. To discover the instant at which the flexible manipulator collides with an unknown obstacle, the innovation of the unscented Kalman filter – a nonlinear state estimator – is introduced. To control the manipulator, a sliding mode controller is employed. Under the normal conditions, the sliding mode controller generates control torques such that the tip position of the manipulator follows a given reference trajectory. However, when collision between the flexible manipulator and an obstacle is detected, the controller switches from position control to suspend control by changing the reference trajectory. The performance of the proposed collision detection algorithm and controller is demonstrated via two numerical simulations.*

Keywords: Unscented Kalman filter, Flexible manipulator, Collision detection, Sliding mode control, Innovation

1. **Introduction.** Recently, flexible manipulators have received increased attention and have been investigated by many researchers [1-6]. In particular it has been desirable to design flexible manipulators having both the features of a lightweight structure and flexibility. As a result, current flexible manipulators have the advantages of being lightweight and having low energy consumption. Such flexible manipulators have useful applications in a number of fields, for example, space development programs and robots for assisting humans. However, derivation of mathematical models and of accurate positioning control is nontrivial for flexible manipulators because they are subject to undesirable vibrations due to their low rigidity.

Furthermore, when utilizing flexible manipulators in a work environment, ensuring the safe operation of the manipulator is important, since there are often a variety of obstacles in the workspace (e.g., objects and humans). Therefore, flexible manipulators

must be able to move while avoiding these obstacles. However, avoidance of unknown obstacles in the workspace is not always possible, and to mitigate damage caused by a flexible manipulator, the introduction of both active collision detection and suspend control algorithms is necessary. Unfortunately, a sensor that detects collisions cannot be installed directly on the manipulator, since this compromises the advantage of having lightweight characteristics. Hence, the development of a collision detection mechanism for the flexible manipulators that is based on observation data is a significant and challenging mission.

Several investigations on collision detection methods for flexible manipulators that do not involve additional sensors have already been conducted [7-9]. Moorehead and Wang proposed a collision detection method for a flexible cantilevered beam by using two strain gauges to determine the intensity and position of the external force resulting from a collision [7]. In their approach, estimation of the contact position was achieved by observing the relation between the positions of the strain gauges and bending moments measured by sensors. One of the current authors also proposed a method of collision detection for a single-link flexible manipulator by using the innovation of a Kalman filter [12, 13]. Furthermore, the authors presented a method of collision detection and suspend control for parallel-structured single-link flexible arms [14]. In that paper, collision is detected by using the innovation of the Kalman filter based on data measure by strain sensors affixed to the side of the arm.

Here, we extend our previously proposed collision detection approach [14] to a parallel-structured two-link flexible manipulator by employing an unscented Kalman filter (UKF) [15], a common nonlinear filter. The advantageous features of the parallel-structured flexible manipulator are that it has sufficient rigidity in the vertical axis and displaying flexibility in the displacement axis of the arm [16]. The mathematical model of the parallel-structured two-link flexible manipulator is described by nonlinear partial and ordinary differential equations having high complexity, because each link of the manipulator consists of a pair of flexible beams that are deformed in parallel. In our research, each link of the parallel-structured two-link flexible manipulator is instead modeled approximately by a single flexible beam under the same boundary conditions as the original system. Collision detection is then realized by using the innovation of the state estimator.

To achieve collision detection and suspend control for the flexible manipulator, we employ the UKF, a nonlinear state estimator proposed by Julier et al. [17-19] and a sliding mode controller. Although linearization of the mathematical model for the parallel-structured two-link flexible manipulator is nontrivial owing to its high nonlinearity, the state estimator for the manipulator can be constructed by using the UKF. The UKF is chosen, since the intensity of the UKF innovation jumps to a large value at the instant a collision occurs. Hence, by introducing a scalar function based on the innovation, collisions between unknown obstacles and the flexible manipulator can be detected if the function exceeds a pre-assigned threshold.

A controller for the nonlinear system model is additionally required. For this purpose, a sliding mode controller is considered suitable for tracking and suspending control of the manipulator. This controller has a simple structure and is robust [20]. When a collision is detected, the controller is switched from tracking control of the tip position to suspend control, which then replaces the reference trajectory at the point where the collision occurred.

2. **Mathematical Model.**

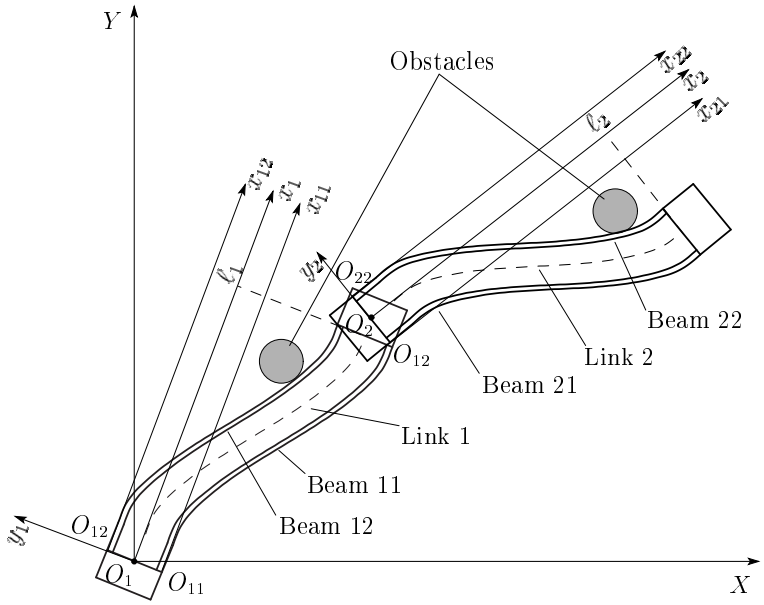

FIGURE 1. Parallel-structured two-link flexible manipulator

2.1. **Parallel-structured two-link flexible manipulator.** Consider a parallel-structured two-link flexible manipulator that collides with unknown obstacles, as schematically illustrated in Figure 1. Each link of the manipulator consists of a pair of uniform Euler-Bernoulli beams. To join the links, one end of each beam is clamped to a hub unit, while the remaining end is clamped to a tip-mass. Under this configuration, for Link i, let O_1XY be the inertial Cartesian coordinate system, $O_ix_iy_i$ $(i = 1, 2)$ be the coordinate systems rotated by servomotors installed at O_1 and O_2, and $O_{ij}x_{ij}y_j$ $(i, j = 1, 2)$ be the rotating coordinate systems of each Beam ij.

Derivation of the mathematical model for the parallel-structured two-link flexible manipulator involves highly complex nonlinear differential equations. However, the principal components of the displacements for Beams $k1$ and $k2$ $(k = 1, 2)$ can be regarded as equal, and assuming that the centripetal force is sufficiently small, the mathematical models for both beams in each link are equivalent. Therefore, for the sake of simplicity, an approximated structure is considered (Figure 2). Here, we consider that each flexible link consisting of two beams is approximated by a single beam under the same boundary conditions as the original system. Hence, each link can be described in terms of a nonlinear partial differential equation.

2.2. **Simple-structured two-link flexible manipulator.** Now, consider the simple-structure two-link flexible manipulator colliding with an unknown obstacle (Figure 2). We assume that the obstacle collides with either Link 1 $(x_1 = x_{c1})$ or Link 2 $(x_2 = x_{c2})$ at time $t = t_c$, where x_{ci} $(i = 1, 2)$ and t_c are all unknown. Let $u_i(t, x_i)$ $(i = 1, 2)$ denote the transverse displacement of Beam i from the x_i-axis and $\theta_i(t)$ be the angle between the O_1X and O_ix_i axes. The physical parameters of the beams are: ρ, the uniform mass density; S, the cross-sectional area; EI, the uniform flexible rigidity (where E is Young's modulus and I is the second moment of cross-sectional area); and c_D, the coefficient of Kelvin-Voigt damping. Furthermore, the hub unit of Link i has moment of inertia J_i, and the tip-mass attached to Link i has mass m_i and moment of inertia J_{i+2}.

The mathematical model for the simplified flexible manipulator can be derived by Hamilton's principle [14], and is given by the following Euler-Bernoulli nonlinear partial

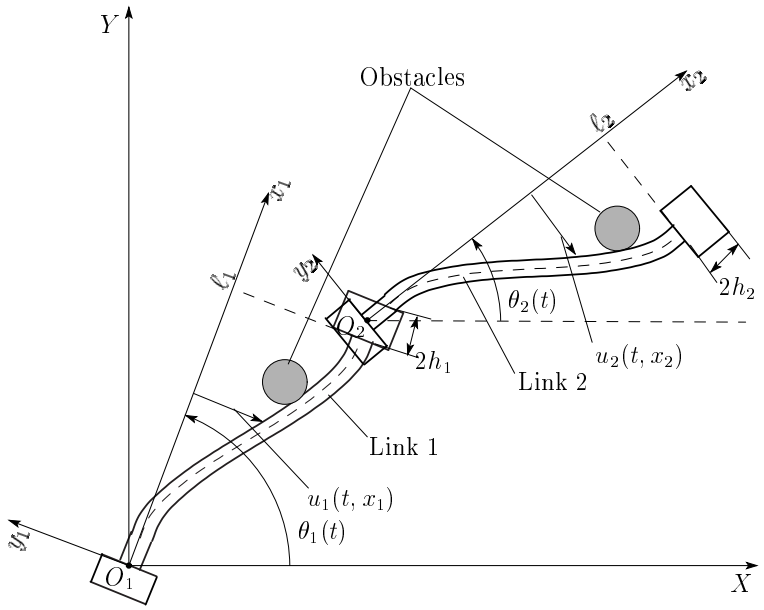

FIGURE 2. Simple-structure model of parallel-structured two-link flexible manipulator

and ordinary differential equations:

$$\begin{aligned}
&\rho S_1\ddot{u}_1(t,x_1) + c_D I_1 \dot{u}_1''''(t,x_1) + EI_1 u_1''''(t,x_1)\\
=&-\rho S_1 x_1 \ddot{\theta}_1(t) + \rho S_1 u_1(t,x_1)\dot{\theta}_1^2(t) + g_1\gamma_1(t,x_1)\\
&+ s_1(t)\delta(x_1 - x_{c1}) - R_1(\mathbf{p})\delta(x_1 - \ell_1),
\end{aligned} \tag{1}$$

$$\begin{aligned}
&\rho S_2\ddot{u}_2(t,x_2) + c_D I_2 \dot{u}_2''''(t,x_2) + EI_2 u_2''''(t,x_2)\\
=&-\rho S_2\Big[\big\{L_1\cos\{\theta_2(t)-\theta_1(t)\} + u_1(t,\ell_1)\sin\{\theta_2(t)-\theta_1(t)\}\big\}\ddot{\theta}_1(t) + x_2\ddot{\theta}_2(t)\\
&+ \ddot{u}_1(t,\ell_1)\cos\{\theta_2(t)-\theta_1(t)\} + \big\{L_1\sin\{\theta_2(t)-\theta_1(t)\}\\
&- u_1(t,\ell_1)\cos\{\theta_2(t)-\theta_1(t)\}\big\}\dot{\theta}_1^2(t) - u_2(t,x_2)\{\dot{\theta}_2(t)-\dot{\theta}_1(t)\}^2\\
&+ 2\dot{u}_1(t,\ell_1)\dot{\theta}_1(t)\sin\{\theta_2(t)-\theta_1(t)\}\Big] + g_2\gamma_2(t,x_2)\\
&+ s_2(t)\delta(x_2 - x_{c2}) - R_2(\mathbf{p})\delta(x_2 - \ell_2),
\end{aligned} \tag{2}$$

$$\begin{aligned}
&P_{11}(\mathbf{p})\ddot{\theta}_1(t) + P_{12}(\mathbf{p})\ddot{\theta}_2(t) + P_{13}(\mathbf{p})\dot{\theta}_1(t) + P_{14}(\mathbf{p})\dot{\theta}_2(t)\\
&+ P_{15}(\mathbf{p})\dot{\theta}_1^2(t) + P_{16}(\mathbf{p})\dot{\theta}_2^2(t) - R_s(\mathbf{p}) + Q_{11}(\mathbf{p})\ddot{u}_1(t,\ell_1) + Q_{12}(\mathbf{p})\dot{u}_1(t,\ell_1)\\
=&\tau_1(t) - \tau_2(t) + g_3\gamma_{\theta 1}(t)
\end{aligned} \tag{3}$$

$$\begin{aligned}
&P_{21}(\mathbf{p})\ddot{\theta}_1(t) + P_{22}(\mathbf{p})\ddot{\theta}_2(t) + P_{23}(\mathbf{p})\dot{\theta}_1(t) + P_{24}(\mathbf{p})\dot{\theta}_2(t)\\
&+ P_{25}(\mathbf{p})\dot{\theta}_1^2(t) + P_{26}(\mathbf{p})\dot{\theta}_2^2(t) + Q_{21}(\mathbf{p})\ddot{u}_1(t,\ell_1) + Q_{22}(\mathbf{p})\ddot{u}_2(t,\ell_2)\\
=&\tau_2(t) + g_4\gamma_{\theta 2}(t),
\end{aligned} \tag{4}$$

where the initial and boundary conditions of (1) and (2) are $u_i(0,x_i) = \dot{u}_i(0,x_i) = 0$ and $u_i(t,0) = u_i'(t,0) = u_i'(t,\ell_i) = u_i'''(t,\ell_i) = 0$ $(i = 1,2)$, and the initial conditions of (3) and (4) are $\theta_i(0) = \theta_{0i}$ and $\dot{\theta}_i(0) = 0$. $\gamma_i(t,x)$ $(i = 1,2)$ represents the distributed random disturbance. $\gamma_{\theta i}$ $(i = 1,2)$ denotes the random disturbance acting at the respective servomotor shaft.

Here, $\mathbf{p}(t) := [\theta_1(t), \theta_2(t), u_1(t, x_1), u_2(t, x_2)]^{\mathrm{T}}$, the prime represents $\partial/\partial x_i$, $L_1 := \ell_1 + h_1$ and g_i $(i = 1, \ldots, 4)$ are constants, $\delta(\cdot)$ denotes the Dirac delta function, and $s_i(t)$ $(i = 1, 2)$ is the magnitude of the collision input. In addition, $P_{ij}(\cdot)$ and $Q_{ij}(\cdot)$ are nonlinear functions, $R_1(\cdot)$ represents the reaction force between the tip-mass and Link 2, $R_2(\cdot)$ is the reaction force of the tip-mass, and $R_s(\cdot)$ is the reaction force resulting from the collision. Finally, $s_i(t)$ $(i = 1, 2)$ denotes the external force due to the collision. Assuming that the collision occurs only momentarily, the magnitude of collision, $s_i(t)$ $(i = 1, 2)$, can be expressed by

$$s_i(t) = s_{i0}\delta(t - t_c), \tag{5}$$

where s_{i0} $(i = 1, 2)$ is unknown parameter.

Observation data are measured with piezoelectric sensors and potentiometers. A piezoelectric sensor with length b_s is affixed at the base of each link $(x_i = \xi_i)$ to measure the strain within the beams. The potentiometers are installed at the shaft of the servomotors. Observations are given by the following manners:

$$y_i(t) = a_i \int_{\xi_i}^{\xi_i + b_s} u_i''(t, x_i)dx_i + b_i\beta_i(t), \tag{6}$$

$$y_{2+i}(t) = a_{2+i}\theta_i(t) + b_{2+i}\beta_{2+i}(t), \quad (i = 1, 2) \tag{7}$$

where a_i and b_i are constants, and $\beta_i(t)$ represents the observation noise modeled by white Gaussian noise.

2.3. **State space model.** By using the modal expansion method, solutions of (1) and (2) can be represented as

$$u_i(t, x_i) \cong \sum_{k=1}^{N} u_{ik}(t)\phi_{ik}(x_i), \quad (i = 1, 2) \tag{8}$$

where N is a sufficiently large positive number. Moreover, $\phi_{ik}(\cdot)$ is the kth eigenfunction (mode function) corresponding to eigenvalue λ_{ik} of the following eigenvalue problem:

$$\frac{EI}{\rho S_i}\frac{d^4}{dx_i^4}\phi_{ik}(x_i) = \lambda_{ik}\phi_{ik}(x_i), \quad (i = 1, 2) \tag{9}$$

with boundary conditions

$$\phi_{ik}(0) = \frac{d\phi_{ik}(0)}{dx_i} = \frac{d\phi_{ik}(\ell_i)}{dx_i} = \frac{d^3\phi_{ik}(\ell_i)}{dx_i^3} = 0, \tag{10}$$

and $u_{ik}(t)$ $(i = 1, 2)$ denotes the modal displacement corresponding also to λ_{ik}.

Introducing the state vector defined by

$$\begin{aligned} v(t) = [&\dot{u}_{11}(t), \cdots, \dot{u}_{1N}(t), \dot{u}_{21}(t), \cdots, \dot{u}_{2N}(t), \\ &u_{11}(t), \cdots, u_{1N}(t), u_{21}(t), \cdots, u_{2N}(t), \dot{\theta}_1(t), \dot{\theta}_2(t), \theta_1(t), \theta_2(t)]^{\mathrm{T}}, \end{aligned} \tag{11}$$

the state space model of the combination of the simple-structure two-link flexible manipulator and observation model is

$$\dot{v}(t) = A(v)v(t) + B(v)f(t) + G_c(v; x_{c1}, x_{c2})s(t) + G(v)\gamma(t), \tag{12}$$

$$y(t) = Cv(t) + E\eta(t). \tag{13}$$

$G_c(v; x_{c1}, x_{c2})$ is a nonlinear function of the state $v(t)$ and collision positions x_{c1} and x_{c2}; $f(t) := [\tau_1(t), \tau_2(t)]^{\mathrm{T}}$; $\gamma(t) := [\gamma_{11}(t), \cdots, \gamma_{1N}(t), \gamma_{21}(t), \cdots, \gamma_{2N}(t), \gamma_{\theta 1}(t), \gamma_{\theta 2}(t)]^{\mathrm{T}}$; $\gamma_{ik}(t) := \int_0^{\ell_i} \gamma_i(t, x_i)\phi_k(x_i)dx_i$; $\eta(t) := [\beta_1(t), \cdots, \beta_4(t)]^{\mathrm{T}}$; $\mathcal{E}\{\gamma(t)\gamma^{\mathrm{T}}(\tau)\} = W\delta(t - \tau)$ and $\mathcal{E}\{\eta(t)\eta^{\mathrm{T}}(\tau)\} = V\delta(t - \tau)$ (where $\mathcal{E}\{\cdot\}$: the mathematical expectation).

3. **Design of UKF.** The state space model described by (12) and (13) is a stochastic nonlinear system with a collision as the input. To control the tip position and to reduce the random vibration of the entire flexible manipulator, information about the state $v(t)$ is required. For these purposes, the UKF for the following collision-free system is employed:

$$\dot{v}_f(t) = A(v_f)v_f(t) + B(v_f)f(t) + G(v_f)\gamma(t), \tag{14}$$

where $v_f(t)$ is the state vector of the collision-free system.

However, the UKF is to be constructed for a discrete-time nonlinear stochastic system, and (14) is a continuous-time system. Therefore, we convert (14) into a discretized version by using a Runge-Kutta method with a time interval of Δt. (13) and (14) are then rewritten:

$$v_f(k+1) = F(v_f(k), f(k), \gamma(k)), \tag{15}$$

$$y(k) = Cv(k) + E\eta(k), \tag{16}$$

for time-step k. $F(\cdot)$ in (15) is the nonlinear function:

$$\begin{aligned} F(v_f(k), f(k), \gamma(k)) =& v_f(k) + \{H_1(v_f(k), f(k), \gamma(k)) \\ &+ H_2(v_f(k), f(k), \gamma(k)) + H_3(v_f(k), f(k), \gamma(k)) \\ &+ H_4(v_f(k), f(k), \gamma(k))\}\Delta t/6, \end{aligned} \tag{17}$$

$$\begin{aligned} H_1(\cdot) &= A(v_f(k))v_f(k) + B(v_f(k))f(k) + G(v_f(k))\gamma(k), \\ H_2(\cdot) &= A(v_f(k))\{v_f(k) + H_1(\cdot)dt/2\} + B(v_f(k))f(k) + G(v_f(k))\gamma(k), \\ H_3(\cdot) &= A(v_f(k))\{v_f(k) + H_2(\cdot)dt/2\} + B(v_f(k))f(k) + G(v_f(k))\gamma(k), \\ H_4(\cdot) &= A(v_f(k))\{v_f(k) + H_3(\cdot)dt\} + B(v_f(k))f(k) + G(v_f(k))\gamma(k). \end{aligned}$$

The UKF algorithm is then summarized by the following three steps:

[Step 1]: The $(4N+4)$-state vector, $v_f(k)$, is approximated by $2(4N+4)+1$ sigma points, $\mathcal{X}_i$, with weight coefficients W_i:

$$\mathcal{X}_0 = \hat{v}_f(k|k), \tag{18}$$

$$W_0 = \frac{\kappa}{n+\kappa}, \tag{19}$$

$$\mathcal{X}_i = \hat{v}_f(k|k) + \left\{\sqrt{(4N+4+\kappa)P(k|k)}\right\}_i, \tag{20}$$

$$W_i = \frac{1}{2(n+\kappa)}, \tag{21}$$

$$\mathcal{X}_{i+4N+4} = \hat{v}_f(k|k) - \left\{\sqrt{(4N+4+\kappa)P(k|k)}\right\}_i, \tag{22}$$

$$W_{i+4N+4} = \frac{1}{2(n+\kappa)}, \tag{23}$$

$$(i = 1, \ldots, 4N+4)$$

where κ is an integer scaling parameter, W_i is the weight coefficient associated with the ith point, and $\left\{\sqrt{(4N+4+\kappa)P(k|k)}\right\}_i$ represents the ith column of matrix U satisfying $M = UU^{\mathrm{T}}$ when $M := (4N+4+\kappa)P(k|k)$. Here, the U is calculated via the incomplete Cholesky decomposition [21].

[Step 2]: Transform each point by using the nonlinear function $F(\cdot)$, and the predicted mean, covariance, and observation; the innovation covariance, $P_{yy}(k+1|k)$; and the cross correlation matrix, $P_{vy}(k+1|k)$, are

$$\mathcal{X}_i(k+1|k) = F(\mathcal{X}_i(k|k), f(k)), \tag{24}$$

$$\hat{v}_f(k+1|k) = \sum_{i=0}^{2(4N+4)} W_i \mathcal{X}_i(k+1|k), \tag{25}$$

$$P(k+1|k) = \sum_{i=0}^{2(4N+4)} W_i \{\mathcal{X}_i(k+1|k) - \hat{v}_f(k+1|k)\} \times \{\mathcal{X}_i(k+1|k) - \hat{v}_f(k+1|k)\}^{\mathrm{T}} + GWG^{\mathrm{T}}, \tag{26}$$

$$\mathcal{Y}_i(k+1|k) = C\mathcal{X}_i(k+1|k), \tag{27}$$

$$\hat{y}(k+1|k) = \sum_{i=0}^{2(4N+4)} W_i \mathcal{Y}_i(k+1|k), \tag{28}$$

$$P_{yy}(k+1|k) = \sum_{i=0}^{2(4N+4)} W_i \{\mathcal{Y}_i(k+1|k) - \hat{y}(k+1|k)\} \times \{\mathcal{Y}_i(k+1|k) - \hat{y}(k+1|k)\}^{\mathrm{T}} + EVE^{\mathrm{T}}, \tag{29}$$

$$P_{vy}(k+1|k) = \sum_{i=0}^{2(4N+4)} W_i \{\mathcal{X}_i(k+1|k) - \hat{v}_f(k+1|k)\} \times \{\mathcal{Y}_i(k+1|k) - \hat{y}(k+1|k)\}^{\mathrm{T}}. \tag{30}$$

[Step 3]: The state estimate and covariance are given by updating the prediction through the linear update rule, which is specified by choosing weights that minimize the mean squared error of the estimate. The update rule is

$$\hat{v}_f(k+1|k+1) = \hat{v}_f(k+1|k) + K(k+1)\{y(k+1) - \hat{y}(k+1|k)\}, \tag{31}$$

$$P(k+1|k+1) = P(k+1|k) - K(k+1)P_{yy}(k+1|k)K^{\mathrm{T}}(k+1|k), \tag{32}$$

where $K(k+1)$ is the Kalman filter gain given by

$$K(k+1) = P_{vy}(k+1|k)P_{yy}^{-1}(k+1|k). \tag{33}$$

4. **Collision Detection Algorithm.** For the flexible manipulator to collide with an unknown obstacle is undesirable, because the collision input, $s(t)$, affects the state of the flexible manipulator as a disturbance. The problem of the collision detection is considered as a recognizing of the instantaneous change from a collision-free system to a system with a collision. This change of systems can be indentified by using observation data measured by the piezoelectric sensors affixed to the base of the links. Specifically, a collision is detected by making a decision as to whether observation data, $y(t)$, is provided by the collision or collision-free model.

To detect rapid changes of the system, the intensity of the innovation is used. The UKF innovation is defined as the difference between the actual observation and the estimated observation from the collision-free system,

$$\mu(k) = y(k) - C\hat{v}_f(k|k), \tag{34}$$

where $\hat{v}_f(k|k)$ is the estimate of $v_f(k)$ and is calculated from the UKF in the previous section. Substituting (16) into (34), we have

$$\mu(k) = Cz(k) + E\eta(k), \tag{35}$$

where $z(k)$ is the estimation error defined by $z(k) := v(k) - \hat{v}_f(k|k)$. If a collision does not occur, the state vector $v(k)$ is equal to $v_f(k)$. However, if a collision does occur, $v(k)$

is then equal to the state vector of the collision model, and $z(k)$ becomes large due to the collision input. To detect the collision, the scalar *collision detection function*, $r(k)$, is introduced:

$$r(k) = \mu^{\mathrm{T}}(k)\mu(k). \tag{36}$$

If $r(k)$ exceeds threshold ε, then a collision has arisen.

5. **Controller Design.** The mathematical model for the flexible manipulator derived in Section 2 is a nonlinear stochastic system. So that the tip position of the flexible manipulator follows a reference trajectory, a controller to generate servomotor control torques is required. In the present study, the sliding mode controller is employed.

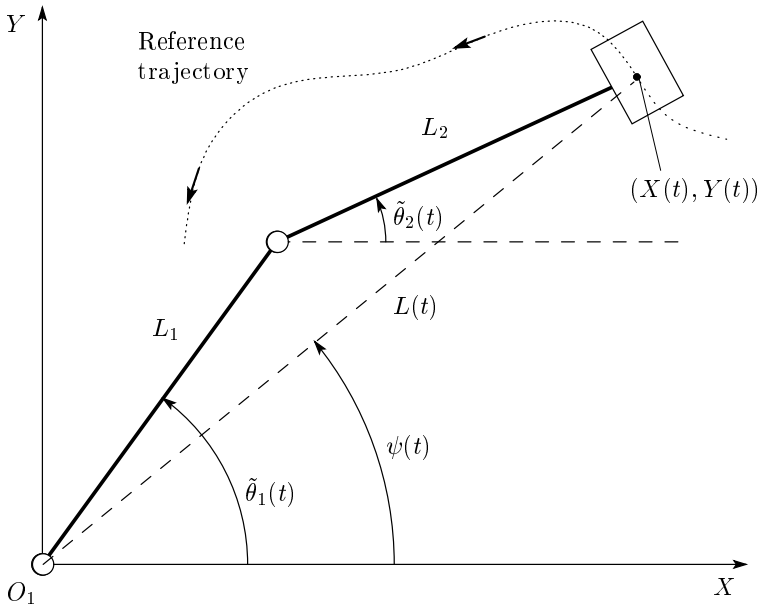

FIGURE 3. The two-link rigid manipulator

5.1. **Error system.** Let us consider that the tip position of a rigid manipulator is moved from an initial position to a desired position on a given reference trajectory, as shown in Figure 3. In this figure, $(X(t), Y(t))$ denotes the tip position of the rigid manipulator. If $\tilde{\theta}_i(t)$ $(i = 1, 2)$ is the reference angle of the joint derived via the inverse kinematics, then

$$\tilde{\theta}_1(t) = \psi(t) + \cos^{-1}\left\{\frac{L^2(t) + L_1^2 - L_2^2}{2L(t)L_1}\right\}, \tag{37}$$

$$\tilde{\theta}_2(t) = \tilde{\theta}_1(t) - \cos^{-1}\left\{\frac{L^2(t) - L_1^2 - L_2^2}{2L_1L_2}\right\}. \tag{38}$$

Here, L_i $(i = 1, 2)$ represents the length of rigid Link i, and $L(t)$ and $\psi(t)$ are given by

$$L(t) = \sqrt{X^2(t) + Y^2(t)} \tag{39}$$

$$\psi(t) = \tan^{-1}\left\{\frac{Y(t)}{X(t)}\right\}. \tag{40}$$

The flexible manipulator is controlled such that its state converges to the equilibrium state given by the rigid manipulator; namely, $v_{eq}(t) := [O_{1\times 4N}, \dot{\tilde{\theta}}_1, \dot{\tilde{\theta}}_2, \tilde{\theta}_1, \tilde{\theta}_2]$, where $O_{1\times 4N}$

expresses the $1 \times 4N$ zero vector. The error state vector, $v_e(t)$, is thus defined by

$$\begin{aligned} v_e(t) &:= v(t) - v_{eq}(t) \\ &\equiv [\dot{u}_{11}(t), \cdots, \dot{u}_{1N}(t), \dot{u}_{21}(t), \cdots, \dot{u}_{2N}(t), \\ &\qquad u_{11}(t), \cdots, u_{1N}(t), u_{21}(t), \cdots, u_{2N}(t), \dot{e}_1(t), \dot{e}_2(t), e_1(t), e_2(t)]^{\mathrm{T}}, \end{aligned} \tag{41}$$

for $e_i(t) := \theta_i(t) - \tilde{\theta}_i(t)$ $(i = 1, 2)$. By introducing $v_e(t)$, the system of errors corresponding to (12) is

$$\dot{v}_e(t) = A(v_e(t))v_e(t) + B(v_e(t))f(t). \tag{42}$$

If the flexible manipulator is precisely controlled, the amplitude of $v_e(t)$ can be regarded as being sufficiently small (i.e., $\|v_e(t)\| \ll 1$). Furthermore, in this paper, we assume that $A(v_e(t)) \cong A(0)$ and $B(v_e(t)) \cong B(0)$. From these approximations, the error system is rewritten as

$$\dot{v}_e(t) = A_e v_e(t) + B_e f(t), \tag{43}$$

where A_e and B_e are the constant matrices defined by

$$A_e := A(0), \quad B_e := B(0). \tag{44}$$

5.2. **Sliding mode controller.** The objective of the sliding mode controller is to track the reference trajectory through the tip position and to suppress any random vibration of the manipulator. Moreover, the controller suspends the motion of the manipulator when a collision is detected.

The input to the controller is given by

$$f(t) = -(SB_e)^{-1} S A_e v_e(t) - F \frac{\sigma(t)}{\|\sigma(t)\| + \delta}, \tag{45}$$

where S is a hyperplane, δ is a positive constant, F is the nonlinear controller gain, and $\sigma(t)$ is a switching function. There are a number of methods for determining the matrix S. Here, S is chosen as a feedback gain of the optimal controller. Explicitly, S is determined as follows [20]:

$$S = B_e^{\mathrm{T}} P, \tag{46}$$

$$P A_e + A_e^{\mathrm{T}} P - P B_e B_e^{\mathrm{T}} P + Q = 0, \tag{47}$$

Q above denotes the non-negative symmetric weight matrix from the cost functional:

$$\begin{aligned} J = \int_0^T \Bigg\{ & \int_0^{\ell_1} \left[q_1 \{\dot{u}_1(t, x_1)\}^2 + q_2 \{u_1(t, x_1)\}^2 + q_3 \{\dot{u}_1''(t, x_1)\}^2 + q_4 \{u_1''(t, x_1)\}^2 \right] dx_1 \\ & + \int_0^{\ell_2} \left[q_5 \{\dot{u}_2(t, x_2)\}^2 + q_6 \{u_2(t, x_2)\}^2 + q_7 \{\dot{u}_2''(t, x_2)\}^2 + q_8 \{u_2''(t, x_2)\}^2 \right] dx_2 \\ & + q_9 \dot{e}_1^2(t) + q_{10} e_1^2(t) + q_{11} \dot{e}_2^2(t) + q_{12} e_2^2(t) \Bigg\} dt \\ \equiv & \int_0^T v_e^{\mathrm{T}}(t) Q v_e(t) dt, \end{aligned} \tag{48}$$

and $Q := \mathrm{diag}\{\Theta_1, \Theta_3, \Theta_2, \Theta_4, q_9, q_{11}, q_{10}, q_{12}\}$; $\Theta_1 = q_1 I_N + q_3 \Psi_1$. Additionally, in this functional, $\Theta_2 = q_2 I_N + q_4 \Psi_1$, $\Theta_3 = q_5 I_N + q_7 \Psi_2$, $\Theta_4 = q_6 I_N + q_8 \Psi_2$ (I_N: N-dimensional

unit matrix), and

$$\Psi_i = \begin{bmatrix} \int_0^{\ell_i} \phi''_{i1}(x_i)\phi''_{i1}(x_i)dx_i, \cdots, \int_0^{\ell_i} \phi''_{i1}(x_i)\phi''_{iN}(x_i)dx_i \\ \vdots \qquad\qquad\qquad \vdots \\ \int_0^{\ell_i} \phi''_{iN}(x_i)\phi''_{i1}(x_i)dx_i, \cdots, \int_0^{\ell_i} \phi''_{iN}(x_i)\phi''_{iN}(x_i)dx_i \end{bmatrix}. \tag{49}$$

Finally, the switching function for the controller input is defined by

$$\sigma(t) = Sv_e(t), \tag{50}$$

and nonlinear controller gain must satisfy the following condition:

$$F \begin{cases} > 0 & : \text{ if } SB_e > 0 \\ < 0 & : \text{ if } SB_e < 0. \end{cases} \tag{51}$$

Because we are using an unscented Kalman filter, the continuous $\sigma(t)$ and $f(t)$ functions given by the sliding mode controller must be discretized using

$$\sigma(k) = Sv_e(k) \tag{52}$$

$$f(k) = -(SB_e)^{-1}SA_ev_e(k) - F\frac{\sigma(k)}{\|\sigma(k)\| + \delta}. \tag{53}$$

5.3. **Suspend control.** When a collision is detected, the flexible manipulator is suspended to absorb the impact of the collision. With the flexible manipulator controlled such that the tip position tracks the reference trajectory, to suspend the motion of the manipulator using the sliding mode controller, we consider that the reference trajectory is switched to an alternative trajectory at t_c when collision occurs. The tip position of the manipulator at t_c is defined by

$$(X(t_c), Y(t_c)) =: (X_c, Y_c), \tag{54}$$

where X_c and Y_c are constants. Suspend control is thus achieved by fixing the reference trajectory at (X_c, Y_c) after the collision has been detected:

$$\begin{cases} X(t) = X_c \\ Y(t) = Y_c \end{cases} \quad (t > t_c) \tag{55}$$

6. **Simulation Results.** In this section, we present the results of two numerical simulations. To this end, the flexible beams are assumed to be composed of phosphor bronze. Physical parameters and coefficients of the flexible manipulator are listed in Table 1. Theoretical observation data are assumed to have been measured with piezoelectric sensors having length $b_s = 3 \times 10^{-2}$ [m] and width 1.2×10^{-2} [m], affixed at positions $\xi_i = 3 \times 10^{-3}$ [m] $(i = 1, 2)$, and potentiometers are installed at the respective hubs. Observation system parameters were set as $a_i = b_i = 1.0$ $(i = 1, \cdots, 4)$. The covariance matrices for the system noise and the observation noise were given by $W = 10^{-5} \times I_{4N+4}$ and $V = 10^{-8} \times I_4$, respectively. The number of modes of the flexible arms was fixed at $N = 2$. Finally, the time partition in the numerical simulations was set as $\Delta t = 1 \times 10^{-3}$ [s].

TABLE 1. Physical parameters of the flexible manipulator

Parameter	Value
ℓ_1	0.3 [m]
ℓ_2	0.28 [m]
E	1.1×10^5 [MPa]
S_1	4×10^{-5} [m^2]
S_2	8×10^{-6} [m^2]
ρ	8.8×10^3 [kg/m^2]
c_D	4.84×10^4 [N·s/m^2]
J_1	0.01 [kg·m^2]
J_2	0.035 [kg·m^2]
J_3	0.035 [kg·m^2]
J_4	0.002 [kg·m^2]
m_1	0.3 [kg]
m_2	0.02 [kg]
h_1	0.04 [m]
h_2	0.01 [m]
g_i $(i=1,\ldots,4)$	1.0

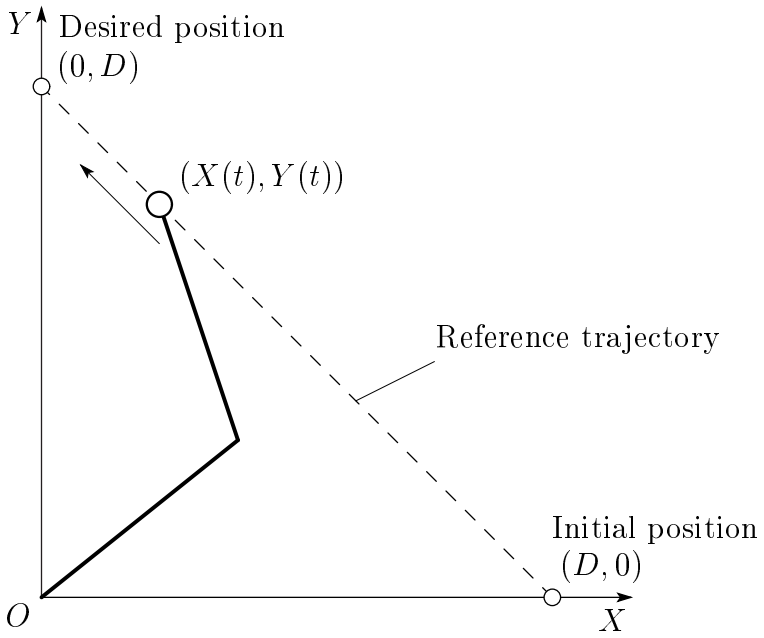

FIGURE 4. Straight-line reference trajectory for the tip of the flexible manipulator

6.1. **Tracking control.** Consider a reference trajectory given by a straight line (Figure 4). If the position at the tip is $(X(t), Y(t))$, then the straight line is defined by

$$X(t) + Y(t) = D, \tag{56}$$

where D $(\leq L_1 + L_2)$ is a positive constant. The tip of the flexible manipulator, therefore, moves to desired position $(0, D)$ from initial position $(D, 0)$. In the simulation, we set $D = 0.5$ [m], and the tip of the flexible manipulator was assumed to reach the desired position at $t = 2$ [s]. Moreover, the initial conditions given to the model were $u_{ij}(0) = 0$ [m], $\dot{u}_{ij}(0) = 0$ [m/s], $\dot{\theta}_i(0) = 0$ [rad/s], $\theta_1(0) = 0.60$ [rad], $\theta_2(0) = -0.72$ [rad], and

the initial condition of the state vector for the control error system was set to zero. The reference angles are calculated from (37)-(40). The weight coefficients in the cost functional were set as $q_1 = 50$, $q_2 = 1000$, $q_3 = 500$, $q_4 = 10$, $q_5 = 500$, $q_6 = 1000$, $q_7 = 500$, $q_8 = 10$, $q_9 = 10$, $q_{10} = 5000$, $q_{11} = 10$, $q_{12} = 5000$. Lastly, the nonlinear controller gain was $F = 1$ and $\delta = 0.5$. The simulation study was carried out for 3 s. The resultant path of the tip mass for the case of the tracking control shown in Figure 5 was computed from

$$X(t) = L_1 \cos\theta_1(t) - u_1(t, \ell_1) \sin\theta_1(t) + L_2 \cos\theta_2(t) - u_2(t, \ell_2) \sin\theta_2(t), \tag{57}$$

$$Y(t) = L_1 \sin\theta_1(t) + u_1(t, \ell_1) \cos\theta_1(t) + L_2 \sin\theta_2(t) + u_2(t, \ell_2) \cos\theta_2(t), \tag{58}$$

where

$$u_i(t, \ell_i) = \sum_{k=1}^{2} u_{ik}(t) \phi_{ik}(\ell_i). \tag{59}$$

As seen in Figure 5, the tip position of the flexible manipulator has almost traced the target trajectory exactly.

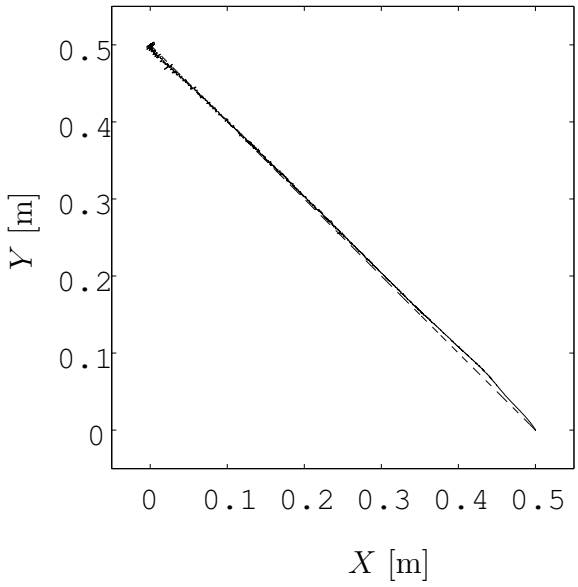

FIGURE 5. Behavior of tip position of the flexible manipulator controlled by the sliding mode controller. In this figure, the dashed line depicts the reference trajectory, and the solid line represents the tip's trajectory of the flexible manipulator calculated from (57) and (58).

6.2. **Collision detection and suspend control.** A numerical simulation of collision detection and suspend control for two-link flexible manipulator was performed. The suspend trajectory for this example was the same as that used in the previous simulation (Figure 4). After the collision was detected, the fixed position was used as the reference trajectory that is given by (55). The collision was assumed to occur at $t_c = 1$ [s] and the threshold was $\varepsilon = 1 \times 10^{-7}$.

The numerical results for the case that the obstacle collides with Link 1 are only considered. Figure 6 shows the variation over time of $r(t)$ $(t = k\Delta t)$. It can be seen that $r(t)$ has risen sharply at $t = 1$ [s]. Hence, the value of the collision detection function exceeded ε at the moment the collision occurred. Figure 7 shows the corresponding trajectory of the tip position. The tip position initially changed significantly due to the input when

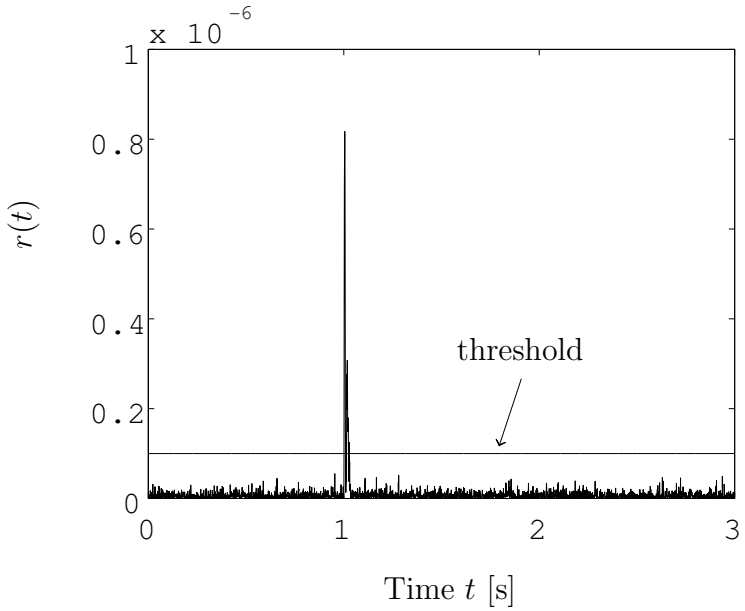

FIGURE 6. Behavior of the collision detection function, $r(t)$, for the case when an obstacle collides with Link 1 ($x_{c1} = 0.15$ [m], $t_c = 1$ [s], $\theta_2(t) = 0$ [rad])

the collision was detected. However, the tip was then suspended at the position that the collision took place.

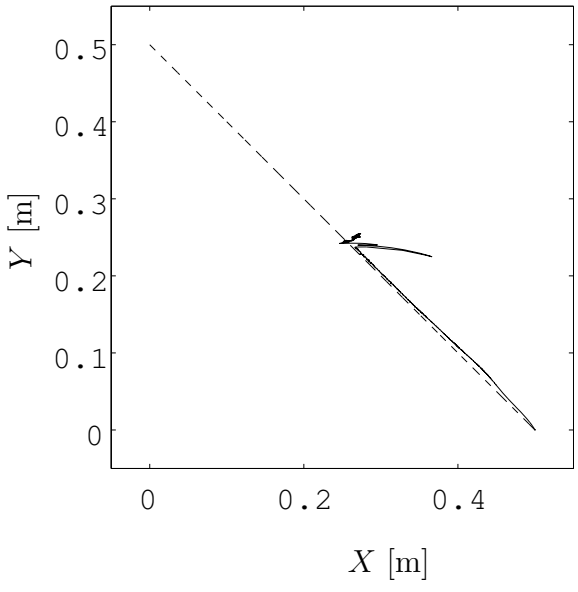

FIGURE 7. Trajectory of the tip position of flexible manipulator when a collision is detected at Link 1 at $t_c = 1$ [s]. The dashed line depicts the reference trajectory, and the solid line represents the resultant path of the flexible manipulator calculated from (57) and (58).

7. **Conclusions.** The mathematical model for a parallel-structured two-link flexible manipulator was described by a nonlinear distributed parameter system. The model of the

manipulator was then converted into a finite-dimensional system by using the modal expansion technique, and the UKF and the sliding mode controller were designed for this system. Collision detection was achieved by using the UKF innovation, since the two-link flexible manipulator is a nonlinear system. Unexpected input caused by a collision with an unknown obstacle excites an undesirable vibration in the flexible manipulator. However, it has been shown that the introduced collision detection function, $r(t)$, successfully detects when a collision has occurred.

The controller for the flexible manipulator was designed via sliding mode control theory. The controller then satisfied the objectives of reducing the random vibration of the flexible manipulator depending on the mechanical flexibility, and controlling the position of the tip-mass such that the tip of the flexible manipulator followed a reference trajectory. Suspend control was also achieved by switching a reference trajectory from the normal control phase to the suspend control phase once the collision was detected.

Performing numerical simulations, the efficiency of the collision detection function and the sliding mode controller were confirmed. Position control of the tip of flexible manipulator has thus been accomplished by using the sliding mode controller.

Garcia et al. [10] investigated a collision detection algorithm based on estimation errors of the arm angle and its derivative, and their approach is similar to our method. However, the mathematical model in their approach is described as a deterministic system. In contrast, since our approach is based on stochastic system theory, collision detection can be achieved even when using a noisy measured signal. This characteristic is realized in that even weak collision impacts could be detected.

Acknowledgment. This research was supported in part by the Japan Society for Promotion of Science (JSPS) under a Grant-in-Aid for Scientific Research (C)-21560240.

REFERENCES

[1] F. Matsuno, T. Asano and Y. Sakawa, Modeling and quasi-static hybrid position/force control of constrained planar two-link flexible manipulators, *IEEE Trans. on Robotics and Automation*, vol.10, no.3, pp.287-297, 1994.

[2] R. N. Banavar and P. Dominic, An LQG/H_∞ controller for a flexible manipulator, *IEEE Trans. on Control Systems Technology*, vol.3, no.4, pp.409-416, 1995.

[3] S.-S. Ge, T.-H. Lee and G. Zhu, Improving regulation of a single-link flexible manipulator with strain feedback, *IEEE Trans. on Robotics and Automation*, vol.14, no.1, pp.179-185, 1998.

[4] M. Bai, D. H. Zhou and H. Schwarz, Adaptive augmented state feedback control for an experimental planar two-link flexible manipulator, *IEEE Trans. on Robotics and Automation*, vol.14, no.6, pp.940-950, 1998.

[5] S. Saito, M. Deng, A. Inoue and C. Jiang, Vibration control of a flexible arm experimental system with hysteresis of piezoelectric actuator, *International Journal of Innovative Computing, Information and Control*, vol.6, no.7, pp.2965-2975, 2010.

[6] Y. Sawada and J. Kondo, Kalman filter based LEQG control of a parallel-structured single-link flexible arm mounted on moving base, *International Journal of Innovative Computing, Information and Control*, vol.6, no.1, pp.29-42, 2010.

[7] S. Moorehead and D. Wang, Collision detection using a flexible manipulator: A feasibility study, *Proc. of IEEE Int. Conf. on Robotics and Automation*, pp.804-809, 1996.

[8] M. Kaneko, N. Kanayama and T. Tsuji, Active antenna for contact sensing, *IEEE Trans. on Robotics and Automation*, vol.14, no.2, pp.278-291, 1998.

[9] T. Matsumoto and K. Kosuge, Collision detection of manipulator based on adaptive control law, *Proc. of 2001 IEEE/ASME Int. Conf. on Advanced Intelligent Mechanics*, pp.177-182, 2001.

[10] A. Garcia, V. Feliu and J. A. Somolinos, Experimental testing of a gauge based collision detection mechanism for a new three-degree-of-freedom flexible robot, *J. Robotics Systems*, vol.20, no.6, pp.271-284, 2003.

[11] I. Payo, V. Feliu and O. D. Cortázara, Force control of a very lightweight single-link flexible arm based on coupling torque feedback, *Mechatronics*, vol.19, no.3, pp.334-347, 2009.

[12] Y. Sawada, On-line collision detection for flexible cantilevered beams using innovation process, *Trans. on ISCIE*, vol.17, no.8, pp.349-357, 2004 (in Japanese).
[13] Y. Sawada, Collision detection and control of a single-link flexible arm, *Trans. on ISCIE*, vol.19, no.6, pp.250-261, 2006 (in Japanese).
[14] J. Kondo and Y. Sawada, Collision detection and suspend control of parallel-structured single-link flexible arms, *Proc. of SICE Annual Conference*, pp.3250-3255, 2008.
[15] M. Yamakita, What is UKF (unscented Kalman filter)? *Systems, Control and Information of ISCIE*, vol.50, no.7, pp.261-266, 2006 (in Japanese).
[16] Y. Sawada and T. Watanabe, LQG control of a parallel-structured single-link flexible arm, *Proc. of the 51th Annual Conference of ISCIE*, pp.372-373, 2007.
[17] S. J. Julier, J. K. Uhlmann and H. F. Durrant-Whyte, A new approach for filtering nonlinear systems, *Proc. of the American Control Conference*, pp.1628-1632, 1995.
[18] S. J. Julier, J. K. Uhlmann and H. F. Durrant-Whyte, A new extension of the Kalman filter to nonlinear systems, *AeroSense: Proc. of the 11th Int. Symp. Aerosp./Defense Sensing, Simulat. Contr.*, Orlando, FL, USA, 1997.
[19] S. J. Julier, J. K. Uhlmann and H. F. Durrant-Whyte, A new method for the nonlinear transformation of means and covariances in filters and estimators, *IEEE Trans. on Automatic Control*, vol.45, no.3, pp.477-482, 2000.
[20] K. Nonami and H. Tian, *Sliding Mode Control: Nonlinear Robust Control Theory*, Corona Pub., 1994 (in Japanese).
[21] Y. Saad, *Iterative Methods for Sparse Linear Systems*, PWS Publishing Company, 1996.